Axial load transfer for piles in sand

III: Load transfer for piles in sand and the critical depth

Ameir Altaee, Erman Evgin, and Bengt H. Fellenius

Department of Civil Engineering, University of Ottawa,
Ottawa, Ontario, Canada, K1N 6N5

ALTAEE, A., EVGIN, E., and FELLENIUS, B. H., 1993. Axial load transfer for piles in sand. III: Load transfer for piles in sand and the critical depth. Canadian Geotechnical Journal, Vol. 30, No. 3., pp. 455 - 463.

Load transfer for piles in sand and the critical depth

AMEIR ALTAEE,[1] BENGT H. FELLENIUS, AND ERMAN EVGIN

Department of Civil Engineering, University of Ottawa, Ottawa, Ont., Canada K1N 6N5

Received May 21, 1992

Accepted February 17, 1993

The authors analyzed the results from a static loading test on a 11.0-m, intrumented, precast concrete pile and presented the findings in two earlier papers. The findings are here extrapolated to verify the dependability of applying the results and analysis methods to predict the detailed behavior of a similar test pile driven 5 m away from the first pile and to a 4.0 m deeper embedment. This paper offers conclusions drawn from the analyses of both piles with regard to residual load and resistance distribution. A primary result of the analyses is the indication that the critical-depth concept is not valid. For full-length piles, the critical-depth concept originates because of neglects in analysis of test data, such as omission of the residual load and testing-sequence history. For tests on short piles and laboratory studies of model piles, a critical depth appears as a result of neglect of the influence of shallow-depth variation of the earth pressure coefficient.

Key words: instrumented piles, sand, loading test, residual load, load transfer, finite element, constitutive modelling, critical-depth concept.

Les auteurs ont analysé les résultats d'un essai de chargement statique sur un pieu instrumenté de 11,0 m en béton préfabriqué et ont présenté les résultats dans deux articles antérieurs. Les résultats sont ici extrapolés pour vérifier le bien-fondé de l'application des résultats et des méthodes d'analyse pour prédire le comportement détaillé d'un essai sur un pieu similaire foncé à 5 m du premier pieu et à un niveau de 4,0 m plus profond. Cet article présente des conclusions tirées des analyses des deux pieux en ce qui concerne le chargement résiduel et la distribution de la résistance. Un premier résultat des analyses indique que le concept de profondeur critique n'est pas valide. Pour les pieux à pleine grandeur, le concept de profondeur critique origine de carences dans l'analyse des données d'essai telles que l'omission du chargement résiduel et de l'histoire de la séquence d'essai. Pour les essais sur des pieux courts et pour les études en laboratoire sur pieux modèles, une profondeur critique apparaît par suite de la négligence de l'influence de la variation à faible profondeur du coefficient des terres au repos.

Mots clés : pieux instrumentés, sable, essai de chargement, chargement résiduel, transfert de charge, élément fini, modélisation de comportement, concept de profondeur critique.

[Traduit par la rédaction]

Can. Geotech. J. **30**, 455–463 (1993)

Introduction

The authors analyzed the results from a static loading test on an instrumented, precast concrete pile (12.0 m long; installed to a depth of 11.0 m) and presented the findings in two papers (Altaee et al. 1992*a*, 1992*b*). As expressed in the first paper, the test results were intended to be used to predict the behavior of piles of different length and size at the site. The first paper included an example of extrapolation of the analysis to the load-movement data of a similar test pile that was driven 5 m away from the first pile and to a 4.0 m deeper embedment. The measured capacity of the longer pile compared well with the calculated capacity obtained by direct application of the effective stress parameters derived from the test on the shorter pile. This paper presents the detailed results of the tests performed on the longer pile and offers some wider conclusions drawn from the analyses.

Soil profile

The soil profile at the site is described in the first of the earlier two papers (Altaee et al. 1992*a*). In summary, the soil consists of an upper, 3.0-m layer of clayey silty sand deposited on a lower, thick layer of uniform sand with some silt. The area is arid, and the groundwater table fluctuates seasonally. At the time of the test now analyzed, i.e., July 1984, the depth to the groundwater table was 6.0 m. Results of standard penetration (SPT) and cone penetrometer (CPT) tests show the soil to be of a compact (medium) condition (N-index values vary from 12 through 25 blows per 0.3 m) and to have an average CPT friction ratio of 2.4%. Additional penetrometer tests, not presented in the papers, show that the soil conditions are laterally very consistent over the about 20 by 15 m large overall test area.

Test piles and instrumentation

The test piles were square, nominally 285 mm diameter, precast concrete piles. The pile reported here (pile 2, 15 m embedment) was built up of one lower 10.0-m segment and one upper 6.0-m segment connected by means of a mechanical splice. Each pile was instrumented with strain gauges, 11 in the spliced, longer pile. The uppermost gauge was placed level with the ground surface to serve as a unit for calibrating measured strain to load in the pile. Pile 1 (11-m embedment) was equipped with eight strain gauges. The earlier paper (Altaee et al. 1992*a*) includes details on the gauges and their calibration.

Pile driving

On June 17 and 18, 1984, in a 15 × 5 m area of the site, several piles were driven by means of a Delmag D12

[1]Present address: Anna Geodynamics Inc., Ottawa, Ont., Canada. K1J 9E2.

Printed in Canada / Imprimé au Canada

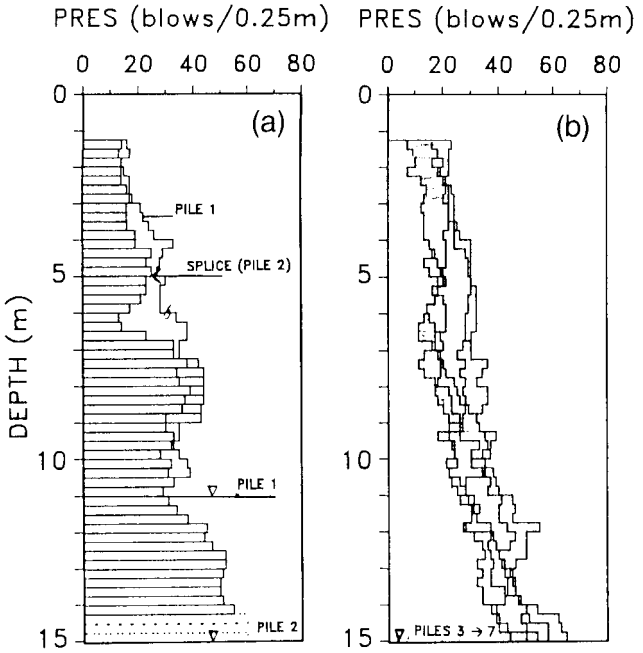

FIG. 1. Pile driving penetration resistance (PRES). (*a*) Piles 1 and 2. (*b*) Piles 3–7.

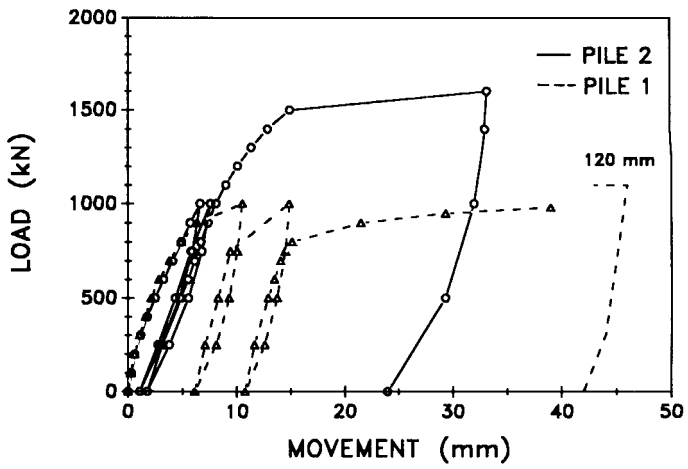

FIG. 2. Pile head load–movement diagram.

diesel hammer. Two of these piles were instrumented and subjected to static loading tests (pile 1, 11.0-m embedment; pile 2, 15.0-m embedment) and five (piles 3–7) were driven to an embedment depth of 15.0 m for the purpose of test driving. Figure 1 presents diagrams over the penetration resistances recorded during the driving. Figure 1*a* shows the penetration resistances (PRES) of piles 1 and 2 in blows per 0.25 m, as recorded. For unknown reasons, the data do not include the pile 2 PRES values for the last 0.75 m of driving. The difference in penetration resistance between the depths of 5.0 and 6.5 m is considered owing to variation of cushion age and hammer performance and not to variations in the soil.

Figure 1*b* shows the distribution of resistance for piles 3–7. Again, the small variations of penetration resistance are considered to be more the result of variations in external factors, such as change in length of use of the hammer cushion, rather than variations in soil density.

Static loading test

On July 15, 1984, 30 days after the end of initial driving (EOID), a static loading test was performed on pile 2. Although the two tests were carried out using the same load levels, the different capacities of the two piles made the tests very different. The load–movement diagram is shown in Fig. 2 and compared with the load–movement diagram of pile 1. Pile 2 was loaded using the same procedure, load levels, and load cycles as used for pile 1: a first cycle of loading the pile in increments of 100 kN to a maximum load of 1000 kN and then unloading. Eight days later, on July 23, this test was repeated. Finally, on July 27, the pile was loaded to failure, which occurred between the applied loads of 1500 and 1600 kN.

As in the case of pile 1, a tension test followed the three compression tests. However, the splice was weaker than the pile uplift strength and broke already at the load of 400 kN (pile 1 had no splice). Therefore, no data of value for load-transfer analysis were obtained from the tension test.

All the strain gauges, but one, resisted the pile driving and exhibited consistent readings during the static loading tests. Figures 3*a*–3*c* portray the load distributions measured during the three tests. The data are presented as recorded, that is, the reading immediately before the start of each test was called "zero" reading. That is, no residual loads before the start of each test are included in the load-distribution diagrams, and the values plotted show only the load at the gauge level due to load applied to the pile head. The load lines marked U1, U2, and U3 indicate the loads in the pile after complete unloading at the pile head for each of the three test cycles (in reference to the zero reading).

Analysis of test data: direct evaluation method

The earlier paper uses effective stress analysis according to the unified method (Fellenius 1989*a*; Goudreault and Fellenius 1990) and applies a direct evaluation method proposed by Fellenius (1989*b*) that simultaneously determines the load distribution in the pile and the residual load present in the pile before the start of the test. From the evaluation of the pile 1 test (first cycle of loading), the effective stress parameters (density, β coefficient, and toe bearing coefficient N_t) applicable to the site were established (Altaee et al. 1992*a*). Complying with the stated intent that the pile 2 test should serve as a verification of the analysis method, these soil parameters were taken unchanged and applied to the conditions for the longer pile (0.2 m higher groundwater table and 4.0 m deeper embedment) to calculate the capacity of the longer pile. This constraint left the matching procedure to work with only the value of the residual toe resistance and the length of the vertical portion of the residual load distribution. The calculation returned the value of 1630 kN, which is very close to the failure range of 1500–1600 kN.

Figure 4 presents the results of the evaluation effort. The open symbols in Fig. 4 represent the measured loads in the pile for the applied load of 1600 kN. At the pile toe, the residual load rises from a residual toe load of about 100 kN in parallel with the calculated true load-distribution line. The vertical portion of the residual

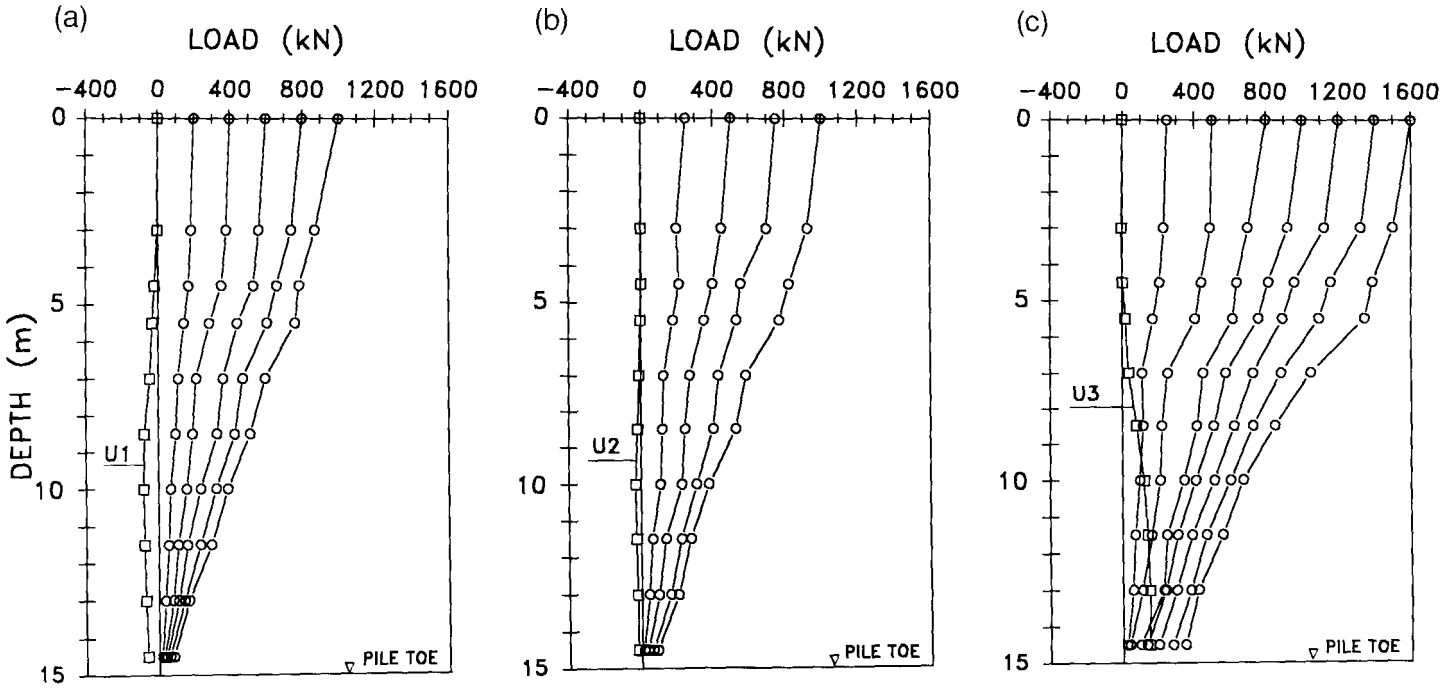

FIG. 3. Load distribution in pile 2 as measured in (*a*) cycle I, (*b*) cycle II, and (*c*) cycle III. Load lines U1, U2, and U3 indicate loads in the pile after complete unloading at the pile head.

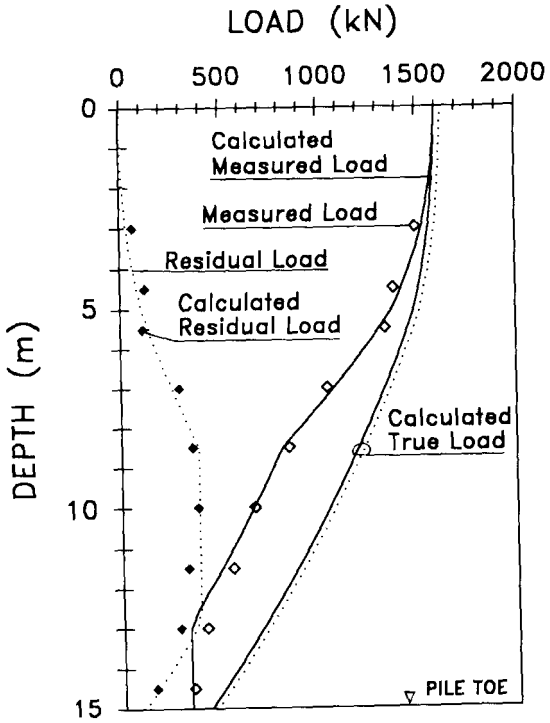

FIG. 4. Load distributions in pile 2 during cycle III as determined by the direct method of analysis.

load-distribution line between the depths of about 9.0 and 13.0 m is the zone of transition from negative skin friction and positive shaft resistance. The residual load is calculated assuming that the negative skin friction is equal to the positive shaft resistance used in the calculation. The solid symbols in Fig. 4 are the residual loads in the pile calculated as the difference between the measured load values and the calculated load distribution.

The residual toe load, 100 kN, is calculated right at the toe of the pile. At the lowest gauge, 0.5 m above the toe, the calculated residual load is about 70 kN larger.

TABLE 1. Maximum load and total shaft and toe resistances by the direct method

Pile No.	Max. load (kN)	Shaft resistance (kN)	Toe resistance (kN)	Cycle
1	1030	670	360	First
2	1630	1160	470	Third

The agreement between the measured loads and the calculated loads is very good, considering the restraints imposed on the analysis. An optimum agreement is achieved by keeping the N_t coefficient of 30 and reducing the β coefficient from 0.65 to 0.60 below the depth of 11.0 m. This change also has the effect of raising the evaluated residual toe load from 100 to about 130 kN. However, the purpose of the analysis is to show the better than acceptable agreement obtained by using the soil parameters "calibrated" from the pile 1 test. Table 1 presents a summary of the results of the direct evaluation method.

It would now be possible to compare the distribution of residual load in piles 1 and 2 and, even, to analyze and compare the load distributions during the first two loading cycles in the two tests. However, the value of such an exercise would be rather debatable. The direct method of analysis has resulted in the following: (*i*) confirmed that the soil conditions at the site are sufficiently uniform to allow an extrapolation to the longer pile; (*ii*) served as a verification that the conventional effective stress method is applicable; (*iii*) proved that the particular β and N_t coefficients of the effective stress method were correctly determined; and (*iv*) showed that the results of the direct method will serve as independent

TABLE 2. Model parameters used in the analysis of piles 1 and 2

Parameter	Value				
	Soil layer				
	I	II (dry)	III (moist)	IV (saturated)	
Effective angle of friction (degrees)					
Compressoin	32	34	34	36	
Extension	32	34	34	36	
Peak	32	34	34	36	
Poisson's ratio					0.3
Aspect ratio					2.0
Hardening parameter					1.0
Critical void ratio at 100 kPa					0.95
Slope of critical line in $e - \ln(p)$ plane					0.05
Unloading–reloading modulus					0.01

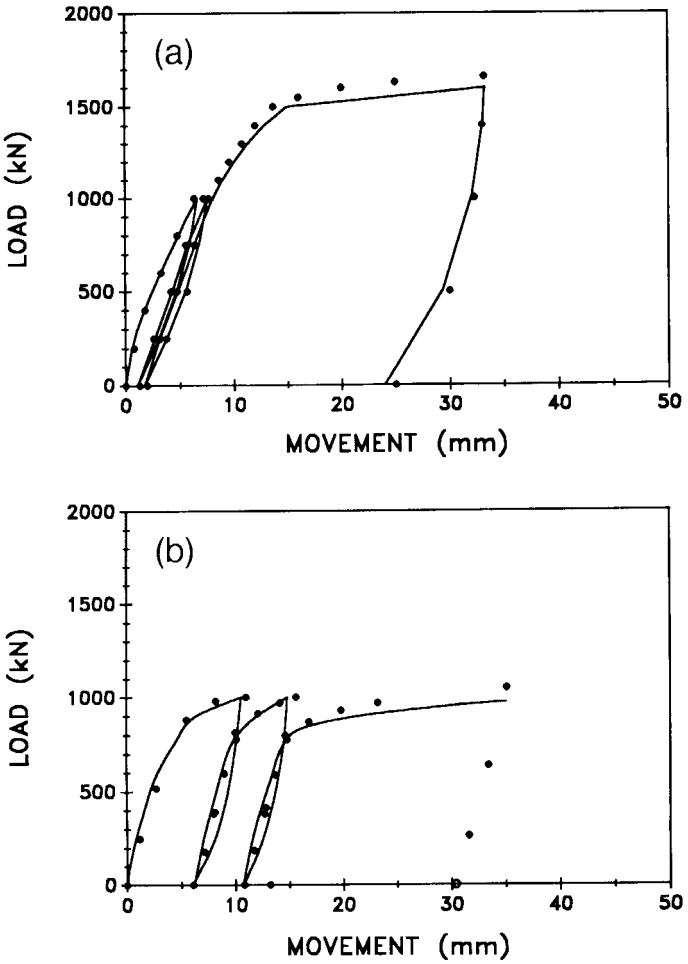

FIG. 5. Applied load vs. pile head movement response; numerical method computation (—) vs. measurements (•). (*a*) Pile 2. (*b*) Pile 1.

reference to the main load distribution determined by means of the numerical method as discussed below.

Analysis of test data: numerical analysis method

Analysis procedure and model parameters

The numerical method was applied to the pile 2 test data, complying, again, with the stated intent that the pile 2 test should serve as a verification of the analysis methods. That is, no new calibration of the parameters was made, but the results of the original calibration of the pile 1 first loading cycle were taken unchanged and applied to the conditions for the longer pile (0.2 m higher groundwater table and 4.0 m deeper embedment). The parameters are listed in Table 2, and further details are contained in Altaee et al. (1992*b*). The computations gave the total capacity, the load–movement, the load distributions for the applied test loads and after unloading to zero load at the pile head, and the residual loads in the pile.

The steps of the analysis are as follows. (*i*) The effect of the installation in terms of load remaining in the pile after the last hammer impact was modeled by imposing downward displacement increments at the pile head until the computed movement values indicated failure, i.e., no increase in resistance between displacement increments. The pile was then unloaded and the resulting elastic rebound of the pile shaft in consort with the rebound of the soil below the pile toe caused the pile to move upward, reversing the direction of forces along the pile, i.e., changing the shear forces from positive shaft resistance to negative skin friction. In this computation, the upper 1.5-m layer of the soil was assumed weightless. (*ii*) To simulate the development of load in the pile after the end of the driving, the weight of the upper 1.5-m layer was introduced, which resulted in a residual load distribution used as the starting point of the simulation of the three cycles of static loading. (*iii*) The load distributions in the pile as a result of each of the two first compression loading cycles were computed by imposing the actual maximum loads of 1000 kN applied in the tests and unloading to zero load at the pile head. (*iv*) To simulate the third loading cycle, the maximum movement of 33 mm was imposed (this movement imposition resulted in a computed maximum load of 1650 kN).

Simulation of load–movement behavior

Figures 5*a* and 5*b* present the simulated load–movement curves for the two static loading tests with comparison to the measured curves. For the pile 2 test, there is a slight overestimation of the capacity: the computed maximum load is 1650 kN at the 33 mm gross pile head movement. However, the overall agreement between measured and computed load–movement is excellent, verifying the

TABLE 3. Test load and total shaft and toe resistances by the numerical method

Pile No.	Test load (kN)	Shaft resistance (kN)	Toe resistance (kN)	Cycle
1	1000	640	360	First
	1000	600	400	Second
	1000	570	430	Third
2	1000	630	370	First
	1000	700	300	Second
	1600	1100	500	Third
	1650	1100	550	Third

method of analysis for determining the capacity of the pile, and also the development of pile head movement due to the imposed load.

Table 3 presents a summary of the results of the numerical method computations of the ultimate shaft and toe resistances for the three test maximum loads. To obtain an additional comparison of the two tests, a separate computation of the load–movement behavior of pile 2 was made of taking the first cycle of load close to the ultimate load, 1600 kN. The computation indicates shaft and toe resistances of 1120 and 480 kN, respectively.

Distribution of residual load

The residual load in the pile is shown in Fig. 6 as computed for the conditions existing immediately before the start of the static loading test. Curve A in Fig. 6 indicates the residual load due to the installation according to step 1 above. Curve R0 is the combined residual load after the residual load additionally induced in step 2 and denotes the residual load just before the start of the static test. The R0 curves suggest that the restraining of the piles occurred both upward and downward from a final equilibrium point located a bit above the pile toe.

The distribution of R0 residual loads is similar in shape for both test piles, as shown in Fig. 7. Three observations can be made from comparing the Fig. 7 distributions of initial residual load in the two piles: (*i*) the relative depth to the neutral plane is about equal for the piles, about 75% of the embedment length; (*ii*) the maximum residual load is larger for the longer pile, pile 2, about 450 kN as opposed to 280 kN for pile 1; and (*iii*) the residual toe load of pile 2 is 300 kN as opposed to 190 kN for pile 1.

The residual load changed as a consequence of each loading cycle. Figure 8 compiles the computed distributions for pile 2. The residual load distribution before the first cycle is denoted R0, and R1, R2, and R3 denote the distributions after unloading for each load cycle. Similar behavior is shown by Altaee et al. (1992*b*) for pile 1.

The first two load cycles to 1000 kN for pile 1 were carried very close to pile failure, inducing significant pile toe penetration, whereas for pile 2 these same loads represented only about 60% of the failure load and very small pile toe penetrations. Therefore, for pile 2, the loading up to 60% of the failure load resulted in a release of the residual load in the pile, whereas for pile 1 the loading close to failure built in additional residual toe load. Loading to failure built in additional residual toe load.

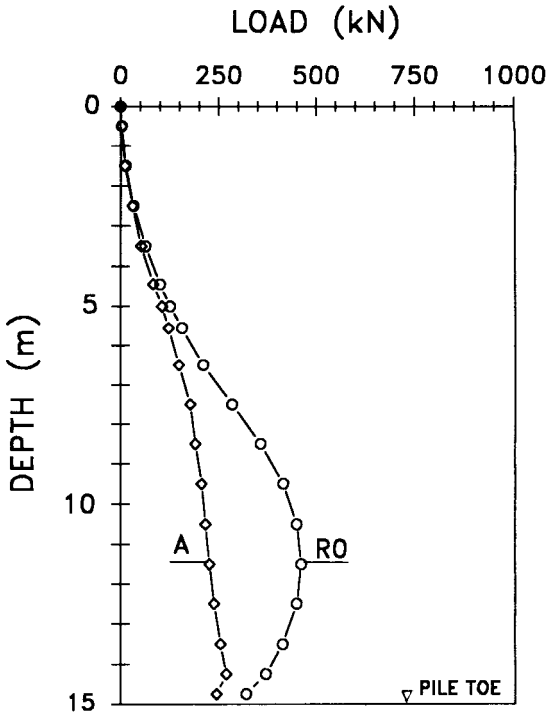

FIG. 6. Steps 1 and 2 installation residual loads of pile 2. Residual load due to loading–unloading (A) and loading–unloading followed by soil vertical compression (R0).

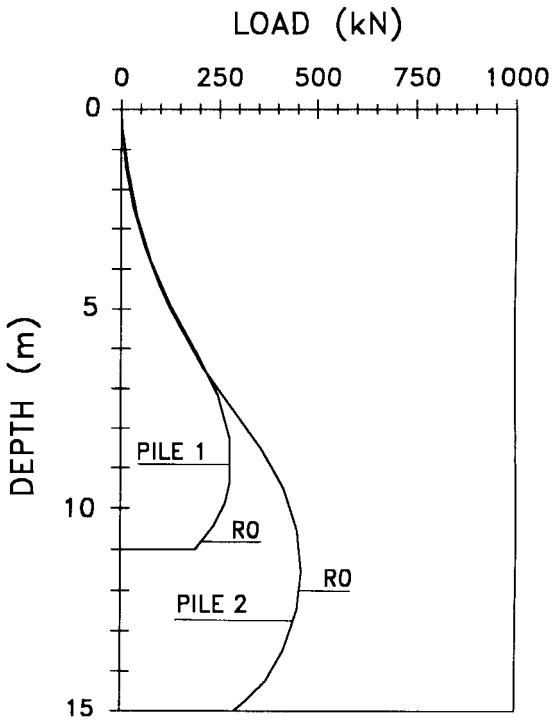

FIG. 7. Distribution of residual load in piles 1 and 2 immediately before cycle I (start of first loading test). R0 is residual load distribution before the first cycle.

The residual toe loads computed in the simulations of the tests are compiled in Table 4. The release of residual load in pile 2, which was subjected to cyclic loading well below the failure load, is in agreement with observations made in laboratory tests performed by Chan and Hanna (1980) and Turner and Kulhawy (1989). In contrast, no such release occurred for pile 1, instead there

TABLE 4. Compilation of computed residual loads before and after test

Pile No.	Test load (kN)	Residual toe load (kN)		Cycle
		Before	After	
1	1000	190	250	First
	1000	250	260	Second
	1000	260	290	Third
2	1000	300	260	First
	1000	260	230	Second
	1650	230	440	Third

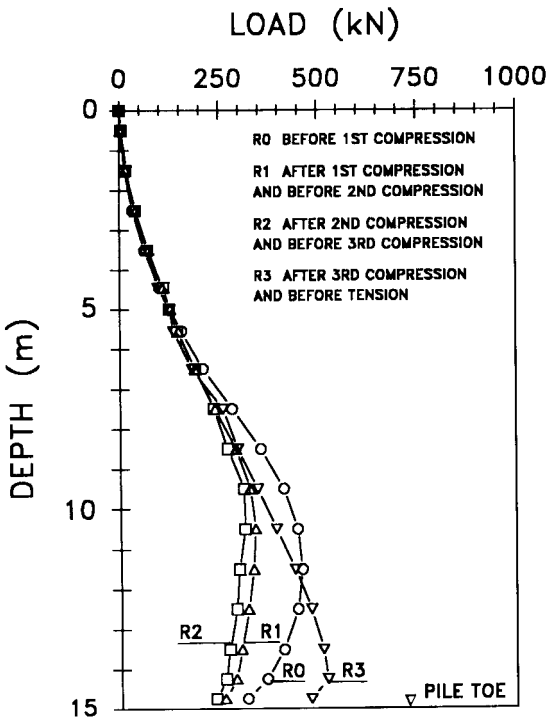

FIG. 8. Effect of loading history on residual load of pile 2.

was an increase. To compare, a separate computation was made for pile 2 of the first cycle of load–movement behavior for the simulation of taking the load beyond 1000 kN and up to 1600 kN, i.e., very close to the failure load, which is the situation for pile 1. This resulted in a residual toe load of 400 kN.

Load distribution

Figures 9*a*–9*c* present the complete load distributions in pile 2 during the three load cycles: (*i*) the computed residual loads before the start of each loading cycle, identified by R; (*ii*) the measured loads at the maximum load applied for each loading cycle, identified by T; (*iii*) the simulated measured loads at the maximum load applied, identified by TP; (*iv*) the computed true loads at the maximum load applied, identified by F, where F = TP + R0.

The agreement between the measured and computed load-distribution curves, T and TP, demonstrates, even more convincingly than the load–movement development of the pile head shown in Fig. 5, that the numerical method has correctly described the behavior of the pile. The additional information that can be gleaned out of the computations consists of distribution of earth pressure coefficient K_f with depth, distribution of unit shaft resistance r_s with depth, and the implication for the so-called critical depth concept as discussed below.

Distribution of earth pressure coefficient

The parameter expressing the earth pressure coefficient at failure, K_f, is used extensively in effective stress analysis of piles (Kulhawy 1984). This coefficient is defined as the ratio of the horizontal effective stress at failure acting against the pile shaft to the initial effective overburden stress. Usually, test results are characterized by a single average value for K_f. The literature shows significant variation of values, ranging from values corresponding to the active earth pressure coefficient through the passive earth pressure coefficient and, numerically, from about 0.1 through about 5.

Figure 10 presents the distribution of the earth pressure coefficient K_f for both piles. The distributions are almost identical for the two piles, i.e., highest near the ground surface, reduced to a relatively constant value along most of the pile shaft, and drastically reduced near the pile toe. When loading the pile, the stress path followed by the soil along the pile shaft is that of simple shear, constant-volume deformation. Near the ground surface, the initial stresses are relatively small and the soil has therefore a higher tendency toward dilatency, i.e., volume increase. The constant-volume constraint, however, results in the development of larger horizontal stress against the pile and a corresponding large value of the earth pressure coefficient K_f. Farther down the pile, the initial effective stresses are larger and, therefore, the tendency toward dilatency is smaller. Consequently, K_f is smaller.

The soil below the pile toe experiences a downward and radial deformation that also affects the soil some distance above the pile toe. Close to the pile toe, the horizontal effective stress against the pile approaches zero. Therefore, the stress path near the pile toe deviates from the simple shear, constant-volume behavior.

The relatively high value of K_f near the ground surface is of little importance for the tests on piles 1 and 2, which are full-scale field tests on full-length piles. However, tests on a very short pile, say 3–4 m in length, would result in high values of average K_f, perhaps somewhat offset by the reduction near the pile toe, whereas the average value for a long pile would be closer to the value along the major portion of the pile. This may explain some of the large variation of the average K_f found in the literature. Furthermore, the analysis results suggest that field tests on short-length piles are performed under nonconstant and nonrepresentative condi-

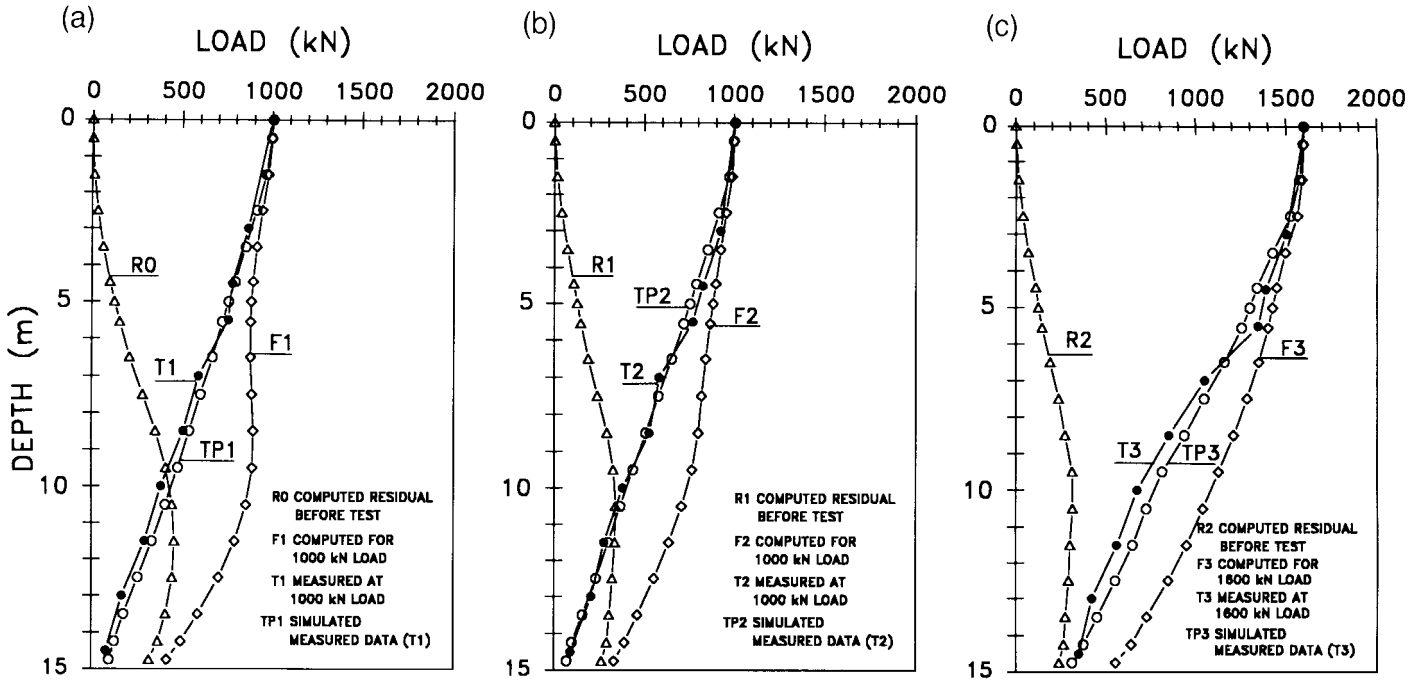

FIG. 9. Distribution of axial load in pile 2. (*a*) Cycle I. (*b*) Cycle II. (*c*) Cycle III.

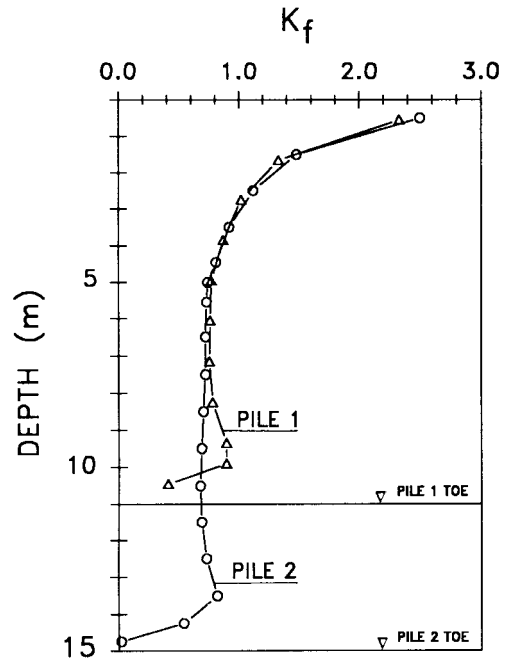

FIG. 10. Computed earth pressure coefficient K_f along piles 1 and 2 at cycle III.

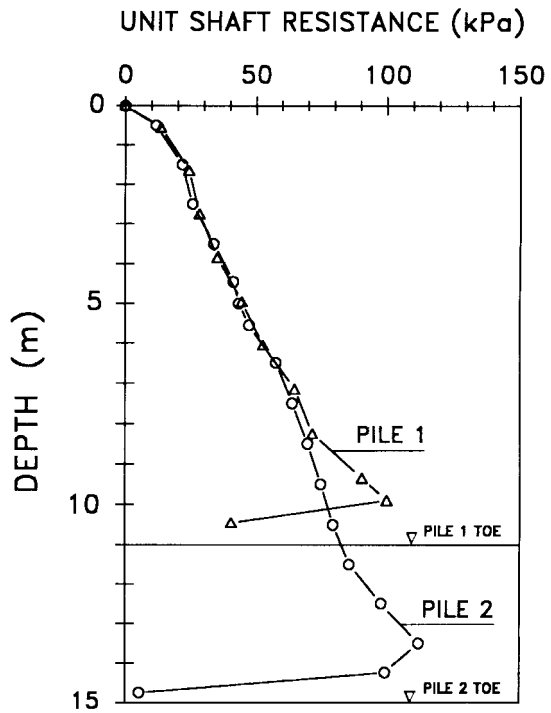

FIG. 11. Distribution of unit shaft resistance in piles 1 and 2 at cycle III.

tions of distribution of the earth pressure coefficient K_f. Therefore, such tests are not directly applicable to the behavior of full-scale piles unless the variation of K_f is considered in the analysis. Of course, tests on laboratory-scale, model piles deviate even more from reality, because the distribution of K_f is not a function of the pile length and, therefore, not of the length to diameter ratio.

Distribution of unit shaft resistance

The effect of the variation of K_f is demonstrated in Fig. 11, which shows the computed distribution of unit shaft resistance r_s, along the pile shaft for the two test piles at failure in the third cycle compression test. For both piles, the unit shaft resistance increases with depth, i.e., is proportional to the effective overburden stress. There is a slight "bulge" near the ground surface due to the increased horizontal stress in this zone. However, because of the relatively small effective overburden stress in the upper portion, the large value of K_f has only a marginal influence on the development of r_s along the two test piles. Near the pile toe, however, the effect of the reduced K_f is one of drastic reduction of the unit shaft resistance at failure.

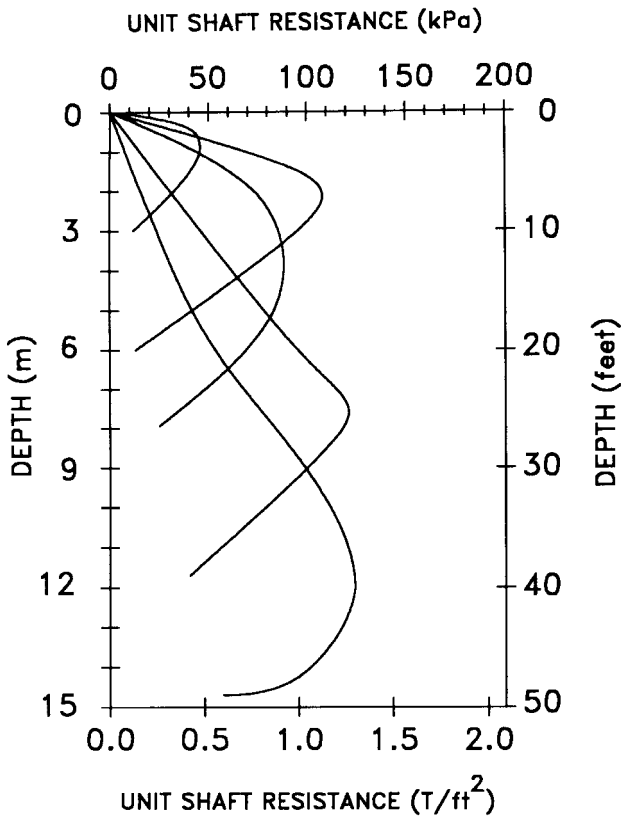

FIG. 12. Distribution of unit shaft resistance according to Vesic (1970).

TABLE 5. Computed toe resistance with and without residual loads

Pile No.	Test load (kN)	Toe resistance (kN)	
		With	Without
1	1000	360	170
2	1600	480	180

Implication for the critical-depth concept

Vesic (1970, 1977) presented results from full-scale field tests which became the main reference to the calculation of shaft and toe resistances for piles. The test results appeared to indicate that a so-called critical depth exists below which the unit shaft and toe resistances would become constant or even diminish with further pile embedment.

Figure 12 shows an evaluation of unit shaft resistances acting on five test piles, published by Vesic (1970). The distributions indicate a reduction of the unit shaft resistance at certain depths and the values, were they to be expressed as a function of β, vary by almost one order of magnitude.

Common for the test results presented in Fig. 12 is that the residual loads were not considered in the evaluation of the data. Nor were the effects of cyclic loading considered when cyclic loading was included in the testing. The residual load acting on the test piles included in Fig. 12 are unknown, of course. However, the importance of including the residual loads in the analysis is demonstrated in the diagram shown in Fig. 13, which includes

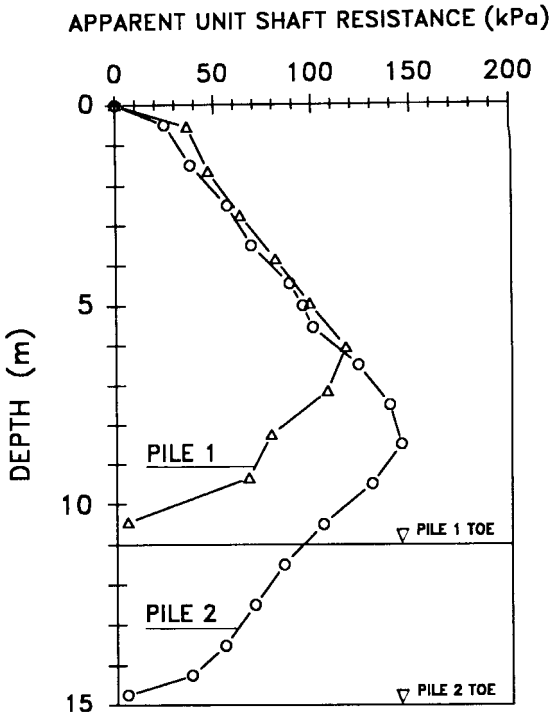

FIG. 13. Distribution of apparent unit shaft resistance of piles 1 and 2 at cycle I when neglecting all residual load in the piles.

the unit shaft resistance computed from the test results from piles 1 and 2 taking the reading at the start of each test as zero, that is, neglecting the residual load in the piles. The similarity with the diagrams in Fig. 12 is obvious, demonstrating that the critical-depth concept of determining shaft resistance is essentially based on a neglect of the effect of the residual load.

According to the critical-depth concept, also the unit toe resistance remains constant below a certain limiting depth value. Researchers have suggested that this depth is a function of the initial soil density and pile diameter (Vesic 1970; Tavenas 1971; Meyerhof 1976). For additional background to the critical-depth concept, see Clemente (1992), Fellenius (1991), Kulhawy (1984), and Kraft (1991). Again, however, the analyses leading up to the finding of the existence of the critical depth do not include residual load. The consequence of this omission is illustrated in Table 5, which shows a comparison of the toe resistances obtained in the computations of the first cycle of compression loading of piles 1 and 2 with and without the residual load prior to the tests.

Conclusions

The results of both the direct method and the numerical method of analysis show that applying the soil parameters developed from the results of the test on pile 1, the shorter pile, closely produces the load distribution and the residual loads acting on the longer pile, pile 2. The numerical method computes a load–movement curve for pile 2 that is close to the observed behavior and accurately computes the degradation of the shaft resistance in cyclic loading.

The numerical method accurately computed the buildup of residual toe load when the cyclic tests are brought close to the ultimate load of the pile and the

release of residual load when the maximum test load is much smaller than the ultimate resistance of the pile. Thus, the numerical method demonstrates the importance of the loading history on the magnitude and distribution of residual load.

When loading the pile, the stress path followed by the soil along the pile shaft is that of simple shear, constant-volume deformation. The tendency toward dilatency near the ground surface (within the upper 2.0–3.0 m), where the effective stresses are small, is larger than at greater depth. Therefore, the computed earth pressure coefficient K_f is larger near the ground surface, and a constant coefficient does not develop until a depth of about 3 m. Near the pile toe, shaft resistance at failure is small, because the horizontal stress against the pile surface is reduced due to radial movement of the soil below the pile toe. That is, in contrast with the situation along the pile shaft, the soil next to the pile is not sheared in simple shear, constant-volume deformation mode.

The authors' analyses indicate that the critical-depth concept is not valid. When the residual loads are removed from the analyses, the distribution of both shaft and toe resistances are similar to that reported from full-scale pile tests supporting the critical-depth concept. The latter tests did not include the residual load in the evaluation. For tests on short piles and laboratory studies of model piles, the critical depth appeared as a result of neglecting the influence of the shallow-depth variation of the earth pressure coefficient.

Acknowledgements

The experimental part of this research was jointly sponsored by the State Contracting Company for Piling and Foundation of Iraq (SCCPF) and the Building Research Center (BRC) of the Iraqi Scientific Research Council. Mr. Hussain U. Bahia and Mr. Ali H. Khalil of the BRC were members of the research team throughout the experimental part of the work. Mr. Safaa Sahib, site engineer of the SCCPF, and Mr. Adil H. Alsaffar, researcher at the BRC, assisted in the laboratory and field preparation. Dr. Laith I. Namiq, Dean of the Engineering College, University of Baghdad, permitted access to the university laboratories. The numerical part of this work was carried out at the University of Ottawa, Department of Civil Engineering, and was financially supported by the Natural Sciences and Engineering Research Council of Canada.

Altaee, A., Fellenius, B.H., and Evgin, E. 1992*a*. Axial load transfer for piles in sand. I. Tests on an instrumented precast pile. Canadian Geotechnical Journal, **29**: 11–20.

Altaee, A., Evgin, E., Fellenius, B.H., 1992*b*. Axial load transfer for piles in sand. II. Numerical analysis. Canadian Geotechnical Journal, **29**: 21–30.

Chan, S.F., and Hanna, T.H. 1980. Repeated loading on single piles in sand. ASCE Journal of the Geotechnical Engineering Division, **106**(GT1): 171–188.

Clemente, J.L.M. 1992. Performance of axially loaded pipe piles in sand. Discussion. ASCE Journal of Geotechnical Engineering, **118**(GT5): 832–835.

Fellenius, B.H. 1989*a*. Unified design of piles and pile groups. Transportation Research Record, **1169**: 75–82.

Fellenius, B.H. 1989*b*. Prediction of pile capacity. *In* Predicted and Observed Behavior of Piles, Proceedings of Pile Prediction Symposium, Evanston, June 1989. *Edited by* R.J. Finno. American Society of Civil Engineers, New York. Geotechnical Special Publication 23. pp. 293–302.

Fellenius, B.H. 1991. Summary of pile capacity predictions and comparison with observed behavior. ASCE Journal of Geotechnical Engineering, **117**(GT1): 192–195.

Goudreault, P.A., and Fellenius, B.H. 1990. Unipile version 1.0 user's manual. Bengt Fellenius Consultants Inc., Ottawa.

Kraft, L.M. 1991. Performance of axially loaded pipe piles in sand. ASCE Journal of Geotechnical Engineering, **117**(GT2): 272–296.

Kulhawy, F.H. 1984. Limiting tip and side resistance: fact or fallacy? *In* Proceedings of the American Society of Civil Engineers, Symposium on Analysis and Design of Pile Foundations. *Edited by* R.J. Meyer. American Society of Civil Engineers, New York. pp. 80–89.

Meyerhof, G.G. 1976. Bearing capacity and settlement of pile foundations. The eleventh Terzaghi lecture. ASCE Journal of the Geotechnical Engineering Division, **102**(GT3): 195–228.

Tavenas, F.A. 1971. Load tests results on friction piles in sand. Canadian Geotechnical Journal, **8**: 7–22.

Turner, J.P., and Kulhawy, F.H. 1989. Load transfer in deep foundations under repeated loading. *In* Proceedings, 1989 Foundation Engineering Congress. *Edited by* F.H. Kulhawy. American Society of Civil Engineers, New York. Vol. 1. pp. 511–525.

Vesic, A.S. 1970. Tests on instrumented piles, Ogeechee River site. ASCE Journal of the Soil Mechanics and Foundations Division, **96**(SM2): 561–584.

Vesic, A.S. 1977. Design of pile foundations. Synthesis of Highway Practice No. 42. National Cooperative Highway Research Program, Transportation Research Board, National Research Council, National Academy of Sciences, Washington.